Internal wave transmission in nonuniform flows

J. T. Nault and B. R. Sutherland[a)]
Department of Mathematical and Statistical Sciences, University of Alberta, Edmonton, Alberta T6C 2G1 Canada

(Received 21 August 2006; accepted 27 November 2006; published online 17 January 2007)

We compute transmission coefficients for internal waves propagating in a fluid with continuously varying stratification and background shear. In stationary fluid the transmission is characterized by the ratio of transmitted to incident energy. More generally, transmission across the shear is appropriately characterized by the ratio of transmitted to incident pseudoenergy flux. First, we examine the transmission and reflection of internal waves incident upon a weakly stratified layer in stationary fluid focusing upon the opposing limits of piecewise-linear theory and a heuristic application of Wentzel-Kramers-Brillouin (WKB) theory. We find the WKB prediction is reasonably accurate if the distance of transition from strong to weak stratification is as small as one sixth the vertical wavelength of the transmitted waves. In the limit of infinitesimally small transition distances the prediction of piecewise-linear theory is reproduced. Second, we consider the transmission of internal waves across a shear layer which initially is uniformly stratified. In particular, we show that significant transmission is possible across critical layers if the minimum gradient Richardson number is less than 1/4. Finally, we show that internal waves can partially transmit across a mixed region that results from the evolution of an unstable shear layer. Transmission across critical layers occurs for waves whose horizontal phase speed matches the background flow speed at levels where the gradient Richardson number is less than 1/4.
 [DOI: 10.1063/1.2424791]

I. INTRODUCTION

Due to the restoring forces of buoyancy, internal waves propagate through fluids having decreasing background density with height, $\bar{\rho}(z)$. Internal waves vertically transport energy in such stably stratified fluids leading to drag and mixing at levels where they break. Previous studies[1,2] have shown that internal waves have a significant effect on ocean mixing. In particular, the "zonal countercurrents," jets with velocity as large as 25 cm s^{-1} observed at depths between 500 m and 3000 m within 2° of the equator,[3] are believed to be driven by internal gravity wave breaking. It has been hypothesized that the waves originate at the base of the surface mixed layer[4–6] or are generated by shear instability of the upper flank of the equatorial undercurrent.[7] It is not well understood how the waves propagate through the background shear and stratification particularly when the background variations are manifest on short scales compared with the vertical wavelength of the waves. Shear instability also results in localized mixing in the ocean. Internal waves may still cross a mixed patch in the presence of a critical layer in shear, but the problem has not been well studied.

Similarly, atmospheric internal waves propagate upward through varying stratification and shear. Internal waves significantly affect the general circulation of the atmosphere.[8,9] But how they do so depends on how they propagate and where they break. In a particular study near Darwin, Australia internal waves were observed in the ionosphere, where they are visualized by OH airglow, presumably originating from a convective storm beneath.[10] Alexander *et al.*[11] performed ray tracing studies that linked internal wave observations at higher altitudes to convective sources in the troposphere. These waves propagated through the mesosphere where they became evanescent. Snively and Pasko[12] proposed that nonlinear wave-wave interactions excited longer-period nonevanescent waves that propagated through the mesosphere and broke in the ionosphere. Walterscheid *et al.*[13] performed numerical simulations using observed background stratification to show that without changing their frequency wave packets were able to penetrate partially through the evanescent region to reach the ionosphere. Generally it is not well understood how internal waves transmit and reflect from the mesosphere when the vertical scale of the waves is comparable to the scale of the background variations.

The purpose of this study is to provide a means with which to predict the transmission and reflection of internal waves through arbitrary background states. In the work presented here, we restrict ourselves to the study of small-amplitude waves in Boussinesq fluid. As such the study is applicable to internal waves in the ocean and to atmospheric waves provided they propagate over distances much smaller than a density scale height. For waves to propagate vertically, the Doppler-shifted frequency

$$\bar{\Omega}(z) \equiv \omega - k\bar{U}(z) \tag{1}$$

must be less than the buoyancy frequency, N. Where $\bar{\Omega} > N$ the waves are said to be evanescent. Here ω is the absolute frequency, k is the horizontal wave number, and $\bar{U}(z)$ is the background horizontal flow. In the Boussinesq approxima-

[a)]Author to whom correspondence should be addressed.

tion $N^2 \equiv -(g/\rho_0)\mathrm{d}\bar{\rho}/\mathrm{d}z$, in which g is the gravitational acceleration and ρ_0 is a characteristic density of the fluid. Here, for convenience, N is given in terms of the background density gradient. Likewise, N can be defined in terms of background potential temperature gradient in a gas.

The calculation of energy and momentum transport for propagating internal waves in media with relatively long vertical variations compared with the vertical wavelength is typically performed using "ray tracing," which applies Wentzel-Kramers-Brillouin (WKB) theory.[14,15] Heuristic arguments suggest that small amplitude waves will reflect from a level where $\bar{\Omega}=N$ and will asymptotically approach a critical level where $\bar{\Omega}=0$.

Applying WKB theory, Lindzen and Barker[16] examined the propagation of internal waves across a critical layer in uniform shear. In their setup waves were generated in a region of high buoyancy frequency, large enough to allow the wave-like propagation, and then propagated through a region of low buoyancy frequency where the waves encountered a critical layer. Beyond this region the buoyancy frequency again became large. They found that the reflected waves could have larger amplitude than the incident waves, suggesting "over-reflection." This study specifically examined waves that resonated with unstable modes and was restricted to hydrostatic waves.

Broutman *et al.*[15] discuss several ray tracing techniques and the limitations introduced by caustics, which occur when rays intersect each other, typically near a reflection level. Caustics may be avoided by making a uniform approximation using Airy functions. Other more advanced techniques involve switching between spatial and wave number formulations near a caustic to "step over" the singularity. Although both these techniques can produce valid solutions, they are limited by the WKB approximations. One purpose of our study is to examine the propagation of waves with arbitrary frequency and wave number.

Resonant energy transfer by internal waves between two localized regions of enhanced stratification representative of the main and seasonal thermocline was described by Eckart.[17] As opposed to theory that invokes the WKB approximation, this study was limited to the examination of modes with vertical wavelength larger than the characteristic height of the ducts and the separation distance between them. Similarly, resonant energy transfer in the atmosphere between the stratosphere and ionosphere was considered by Fritts and Yuan.[18] This study included anelastic effects and background shear. In both cases the modes periodically transferred energy back and forth between the two ducts.

Our study poses no such restrictions; the vertical wavelength of the incident and transmitted waves is arbitrary and we focus upon the one-way transport of energy across an arbitrarily specified background stratification and mean flow.

This work extends the results of Sutherland and Yewchuk,[19] who derived formulae that predicted the one-way transport of energy by waves across a weakly stratified layer. They termed this phenomena "internal wave tunnelling." In their study they generated waves in a stationary flow with uniform stratification surrounding a finite-depth region of lower or zero buoyancy frequency, a structure they termed an "N^2-barrier." Heuristic arguments from WKB theory suggest that waves would completely reflect upon reaching the N^2-barrier. However, this was not the case—significant amounts of wave energy could penetrate the barrier so long as the barrier depth was sufficiently small compared to the wavelength of the internal waves.

These results were extended further by Brown and Sutherland[20] who considered the transmission of waves across a critical layer in a piecewise-linear shear flow embedded within a locally unstratified layer. They found that for relatively strong shear it was possible for internal waves to propagate through critical levels. As the flow was locally unstratified, and the buoyancy frequency thus zero, the gradient Richardson number at the critical level was zero. In the current study, we extend the result of Brown and Sutherland to include transmission across a critical layer where the gradient Richardson number is nonzero.

Eltayeb and McKenzie[21] also examined the transmission of waves across a critical layer in piecewise-linear shear. However, they introduced a hydrostatic approximation to obtain their analytic solution.

Analytic solutions exist for nonpiecewise linear background density and flow profiles. Using hypergeometric functions and neglecting the curvature of the background flow, Van Duin and Kelder[22] considered the transmission of waves across a hyperbolic tangent shear layer with constant buoyancy frequency for large Richardson number. Their physical profiles are examined in Sec. IV and transmission characteristics found using the complete linear wave equation for small Richardson number flows. In the current study we develop a numerical technique that computes the transmission and reflection of internal waves in an arbitrary background buoyancy frequency and shear profiles.

In Sec. II we discuss the theoretical background and numerical methods used to compute internal wave propagation, transmission, and reflection. In Sec. III we apply the code to a continuously varying stratification where waves propagate from a strongly stratified to weakly stratified region and we compare the results with predictions of WKB and piecewise-linear theory. In Sec. IV we examine the effects of a continuously varying background shear in uniformly stratified flow. In Sec. V we consider the same problem but first allow the unstable background flow considered in Sec. IV to evolve nonlinearly to a quasisteady state consisting of a broader shear profile and locally reduced stratification resulting from mixing. Conclusions are provided in Sec. VI.

II. NUMERICAL METHODS

We restrict our consideration to small-amplitude two-dimensional internal waves propagating through a nonrotating inviscid Boussinesq fluid. We assume that incident waves move upward from a vertical level z_0 and can partially transmit through the flow above this level with the outgoing wave amplitude measured at $z_1 > z_0$. Assuming the waves are horizontally periodic with fixed absolute frequency, the wave structure can be represented in terms of the real part of the stream function given by $\psi = \phi(z)\exp[i(kx-\omega t)]$. The

corresponding horizontal and vertical velocity fields are $u=-\partial\psi/\partial z$ and $w=\partial\psi/\partial x$, respectively. The stream function amplitude, ϕ, is given by the solution of the Taylor-Goldstein equation[23]

$$\phi'' + k^2\left(\frac{N^2}{\bar{\Omega}^2} + \frac{\bar{U}''}{k\bar{\Omega}} - 1\right)\phi = 0. \tag{2}$$

Given values of ϕ and ϕ' at z_0, it is possible to integrate Eq. (2) and to determine ϕ everywhere.

The equation is solved numerically using Stoermer's rule[24] whenever $\bar{\Omega}$ is sufficiently large. Near a critical layer $\bar{\Omega}$ is close to zero and the Stoermer method fails. Indeed, if the gradient Richardson number,

$$\mathrm{Ri}_g(z) \equiv \frac{N^2(z)}{(\bar{U}'(z))^2}, \tag{3}$$

exceeds 1/4 at the critical level, then according to ray theory the waves asymptotically approach this level, neither reflecting nor transmitting across it.[14] Although a more rigorous treatment of linear theory allows for transmission across a critical layer with $\mathrm{Ri}_g > 1/4$, waves near the singularity develop rapid vertical oscillations which lead to efficient wave dissipation. Thus we only consider solutions in circumstances for which Ri_g is less than 1/4. Whenever the coefficient in parentheses that precedes the ϕ term in Eq. (2) is smaller in magnitude than 10^{-4} the numerical solver jumps over the singularities using the approximate analytic solution found by the method of Frobenius (see the Appendix). The solver then continues integrating using the Stoermer method.

We must still determine the values of $\phi(z_0)$ and $\phi'(z_0)$ that appropriately describe the transmission and reflection of incident upward-propagating waves. The values of $\phi(z_0)$ and $\phi'(z_0)$ are a superposition of the stream function amplitudes of the incident and reflected waves. At z_0 the value of ϕ is explicitly found as

$$\phi_n(z_0) = A_n \exp(-im_0 z_0) + B_n \exp(im_0 z_0), \tag{4}$$

where $n=1,2$ is an index for a particular guess of the (generally complex) amplitudes A_n and B_n of the incident and reflected waves, respectively. In Eq. (4), m_0 is the vertical wave number at $z=z_0$ which, using Eq. (2) is given by

$$m_0 = k\sqrt{\frac{N^2(z_0)}{\bar{\Omega}^2(z_0)} - 1}. \tag{5}$$

For arbitrary A_n and B_n the structure of ϕ near the top of the domain, at $z=z_1$, is described by the superposition of upward and downward propagating waves. Thus we can write

$$\phi_n(z_1) = C_n \exp(-im_1 z_1) + D_n \exp(im_1 z_1), \tag{6}$$

in which C_n and D_n are the (generally complex) amplitudes of the upward and downward propagating waves, respectively, and

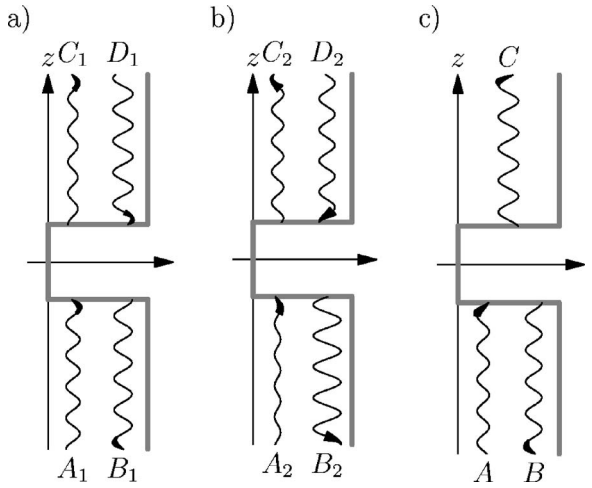

FIG. 1. Schematic illustration of how solutions are superimposed to generate transmission coefficients. (a) Incoming and reflected wave amplitudes A_1 and B_1 are arbitrarily selected, outgoing and returning wave amplitudes C_1 and D_1 are calculated. (b) Different arbitrary amplitudes A_2 and B_2 are selected, and C_2 and D_2 are found. (c) By superimposing the first two solutions, correct amplitudes A and B are calculated such that $D=0$ resulting in transmitted amplitude C and no downward propagating wave incident from above.

$$m_1 = k\sqrt{\frac{N^2(z_1)}{\bar{\Omega}^2(z_1)} - 1}. \tag{7}$$

As (4) and (6) are exact only when $\bar{U}$ and N are constant, the profiles are extended beyond z_0 and z_1 to include regions of constant m_0 and m_1. This is equivalent to our assumption that the incident and reflected stream functions represent monochromatic plane waves.

By causality only upward-propagating waves should occur. Thus we seek a choice of A_n and B_n that ensures $D_n=0$. To determine this correct choice, a first guess is made for A_1 and B_1 and hence, using Eq. (4), for $\phi_1(z_0)$. Equation (2) is solved to find the resulting value of $\phi_1(z_1)$ and hence C_1 and D_1 (which is nonzero for our incorrect initial guesses A_1 and B_1). This is illustrated in Fig. 1(a). The process is repeated by making a new guess for the incident and reflected wave amplitudes A_2 and B_2, respectively, and integrating to determine C_2 and D_2, as illustrated in Fig. 1(b). Because the system is linear, we may superimpose the two initial guesses so as to eliminate D and thus remove downward propagating waves at the top of the domain, this is illustrated in Fig. 1(c). Explicitly, the appropriate choices for A and B are given by

$$A = \frac{A_1}{D_1} - \frac{A_2}{D_2} \quad \text{and} \quad B = \frac{B_1}{D_1} - \frac{B_2}{D_2}. \tag{8}$$

For a prescribed incident amplitude, A, we thus determine the reflected and transmitted wave amplitudes B and C. In the absence of shear, the transmission coefficient is defined as the ratio of squares of the transmitted to incident amplitude[19]

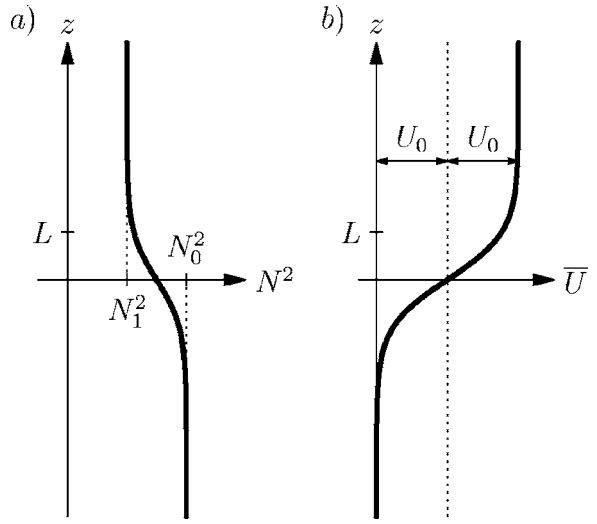

FIG. 2. (a) Schematic illustration of the squared buoyancy frequency profile used for analysis in Sec. III. $\bar{U}=0$ in this case. (b) Schematic illustration of the background horizontal flow used for analysis in Sec. IV. $N^2=N_0^2$ in this case.

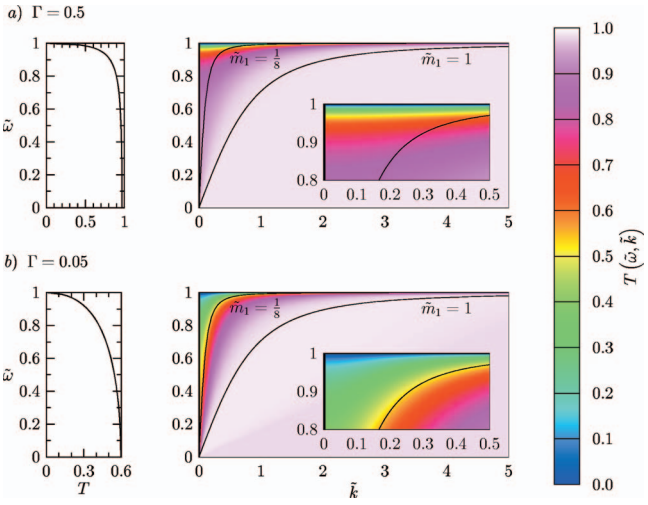

FIG. 3. (Color) Transmission coefficient, T, as a function of incoming wave frequency scaled by incident buoyancy frequency, and wave number scaled by characteristic transition length for (a) $N_1^2=0.5$ and (b) $N_1^2=0.05$. Right plots show contours of T for a range of $\tilde{\omega}$ and $\tilde{k}$. Inset shows close-up of transmission for large frequency and small wave number. Left plots show the analytic solution as $\tilde{k}$ tends to zero.

$$T = \left| \frac{C}{A} \right|^2. \tag{9}$$

This is equivalent to the ratio of transmitted to incident energy density associated with the waves,

$$E = (k^2 + m^2)|A_\psi|^2, \tag{10}$$

for waves with stream function amplitude A_ψ. Likewise the reflection coefficient is defined by

$$R = \left| \frac{B}{A} \right|^2. \tag{11}$$

By conservation of energy, $T+R=1$ must be satisfied.

In the presence of a mean horizontal background flow, wave energy is not conserved due to interactions between the Reynolds stress and the background shear.[20] For small amplitude waves, the appropriate corresponding conserved quantity is wave action,[14,25] $\mathcal{A}=E/\Omega$. Equivalently, as derived using the methods of Hamiltonian fluid mechanics, the so-called pseudoenergy[26,27] of internal waves $\mathcal{E}=\omega E/\bar{\Omega} = \omega\mathcal{A}$ is conserved. So that there is no gain or loss of pseudoenergy in the domain, the transmitted pseudoenergy flux $\mathcal{F}_\mathcal{E}=\mathcal{E}c_{gz}$ must equal the sum of the pseudoenergy flux of the incident and reflected waves. Here c_{gz} is the vertical group velocity given by

$$c_{gz} = -\frac{\bar{\Omega}m}{k^2+m^2}. \tag{12}$$

Thus we define the transmission coefficient in general to be

$$T = \frac{\mathcal{F}_1}{\mathcal{F}_0} = \left| \frac{C}{A} \right|^2 \frac{m_1}{m_0}, \tag{13}$$

and the reflection coefficient is defined as in Eq. (11). In the special case in which $m_1=m_0$, Eq. (13) reduces to Eq. (9).

The code was tested by comparing numerically computed transmission coefficients with analytic results for an N^2 barrier in stationary fluid[19] and in shear.[20] Integrating over 1000 grid points, a typical desktop computer requires about 1 s of computation time to calculate the transmission coefficient for a single set of parameters. Examining transmission for a large range of ω-k space at high (300×300) resolution takes about a day. Typical deviations between the two methods were negligible with maximum transmission coefficient discrepancy less than 1% over a broad range of input ω and k except when critical layers were encountered in which case deviations in the two results were as large as 5%. The larger discrepancy can be explained by the approximations introduced by the method of Frobenius. The error can be improved by increasing the resolution of the numerical integration at the cost of computation time.

III. STATIONARY FLUID RESULTS

We first restrict our study of internal wave transmission to a nonuniformly stratified but stationary fluid. The buoyancy frequency profile is

$$N^2(z) = \frac{N_1^2 - N_0^2}{2} \tanh\left(\frac{z}{L}\right) + \frac{N_0^2 + N_1^2}{2}, \tag{14}$$

as illustrated in Fig. 2(a). We consider internal waves originating from $z_0 \ll 0$, where $N \approx N_0$, and travelling upwards past the step to $z=z_1 \gg 0$, where $N \approx N_1$.

WKB theory at leading order predicts perfect transmission if $\omega < N_1$ and no transmission if $\omega > N_1$. We calculate the transmission coefficient for a range of nondimensional frequencies $\tilde{\omega}=\omega/N_1$ and nondimensional horizontal wave numbers $\tilde{k}=kL$ in circumstances for which $\Gamma \equiv N_1^2/N_0^2=0.5$ and 0.05. The corresponding computed transmission coefficients are plotted in Fig. 3. The transition between the WKB and non-WKB regime is illustrated by lines of constant non-

dimensional transmitted vertical wave number $\tilde{m}_1 \equiv m_1 L = 1$ and 1/8, as determined from the dispersion relation for internal waves:

$$\tilde{\omega} = \frac{\tilde{k}}{\sqrt{\tilde{k}^2 + \tilde{m}_1^2}}. \tag{15}$$

Consistent with the WKB approximation, near-perfect transmission is observed for $\tilde{m}_1 \gg 1$. Surprisingly, the approximation is satisfactory even for $\tilde{m}_1 \approx 1$ corresponding to a transition depth, L, approximately 1/6 of the vertical wavelength of the transmitted waves. Significant departure from the approximation occurs for $\tilde{m}_1 \lesssim 1/8$.

In the limit as $L \to 0$ the smooth profile becomes a step at $z=0$ and the transmission coefficient is found analytically using matching conditions at the step:[19,20,23]

$$T = \left[1 + \frac{1}{4} \left(\sqrt[4]{\frac{(1/\Gamma) - \tilde{\omega}^2}{1 - \tilde{\omega}^2}} - \sqrt[4]{\frac{1 - \tilde{\omega}^2}{(1/\Gamma) - \tilde{\omega}^2}} \right)^2 \right]^{-1}. \tag{16}$$

This is plotted in the left panels of Fig. 3. Comparing the analytic results to those found numerically for $\tilde{k} \approx 0$ we find excellent agreement.

Comparing the transmission contour plots for $\Gamma = 0.5$ and 0.05, there is a clear trend: decreasing Γ decreases the relative transmission for fixed $\tilde{m}_1$. As Γ is reduced the contours of constant T approach lines of constant $\tilde{m}_1$ for sufficiently large $\tilde{k}$. For example, Fig. 3(b) shows that the $\tilde{m}_1 = 1/8$ contour closely corresponds to $T \approx 0.5$ for a range of $\tilde{k} > 0$. Thus wave propagation into weakly stratified fluid is strongly dependent on the transmitted wave vertical wave number.

IV. SHEAR RESULTS

We now examine the effects of background shear in the transmission of internal waves across a region of constant density gradient. In this study the background shear is

$$\bar{U}(z) = U_0 \tanh\left(\frac{z}{L}\right) + U_0, \tag{17}$$

and the buoyancy frequency is constant: $N^2(z) = N_0^2$. The background shear profile is drawn schematically in Fig. 2(b). The strength of the shear relative to the buoyancy frequency is described by the bulk Richardson number,

$$\mathrm{Ri}_b \equiv \left(\frac{N_0 L}{U_0} \right)^2. \tag{18}$$

We now nondimensionalize the frequency, $\tilde{\omega} = \omega / N_0$; horizontal wave number $\tilde{k} = kL/\sqrt{\mathrm{Ri}_b}$; vertical wave number $\tilde{m} = mL$; depth, $\tilde{z} = z/L$; background shear, $\tilde{U} = \bar{U}/U_0$; buoyancy frequency, $\tilde{N} = N/N_0$; and Doppler-shifted frequency, $\tilde{\Omega} = \Omega / N_1$.

Here we focus upon values of Ri_b lying in the range $0 < \mathrm{Ri}_b \leq 1$. In Sec. V, transmission coefficients that are computed for background profiles resulting from the nonlinear evolution of the unstable flow are similar to those computed in this section. This suggests that the evolution of the shear layer has negligible influence upon wave propagation across the layer.

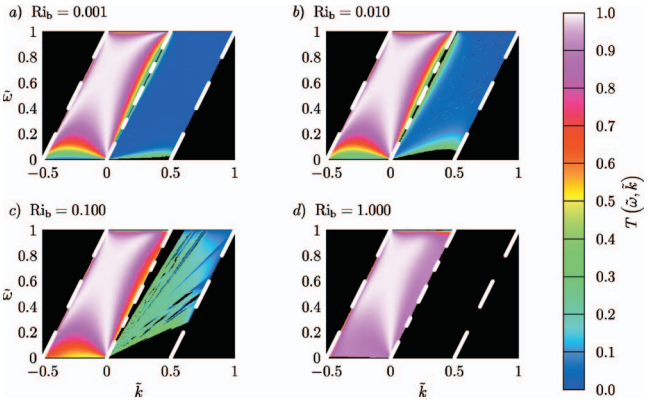

FIG. 4. (Color) Transmission as a function of incoming wave frequency, scaled by N_0, and wave number, scaled by the root of the bulk Richardson number, for (a) $\mathrm{Ri}_b = 0.001$, (b) $\mathrm{Ri}_b = 0.010$, (c) $\mathrm{Ri}_b = 0.100$, and (d) $\mathrm{Ri}_b = 1.000$. To the left of the leftmost line and to the right of the rightmost dashed line wave propagation is not possible at large depths. The center dashed-dotted line marks the boundary between waves that do not encounter a critical layer, to the left of the line, and waves that do encounter a critical layer, to the right of the line.

In each of the four cases considered ($\mathrm{Ri}_b = 0.001$, 0.01, and 1) we set $L=1$ and $U_0=1$. The resulting transmission coefficients, over the range of all frequency and wave number that allow wave-like propagation, are illustrated in Fig. 4. Requiring propagating waves at $\tilde{z}_0$, we restrict $\tilde{\omega} \leq 1$. The plots are divided into four regions: to the left of the leftmost dashed line [where $\tilde{\Omega}(\tilde{z}_1) = \tilde{\omega} - 2\tilde{k} = 1$] and to the right of the rightmost dashed line [where $\tilde{\Omega}(\tilde{z}_1) = -1$] the Doppler-shifted frequency exceeds the buoyancy frequency at $\tilde{z}_1 \gg 0$, and so propagation is not possible. The region between the leftmost dashed line and the dashed-dotted line [where $\tilde{\Omega}(\tilde{z}_1) = 0$] corresponds to wave number and frequency pairs that do not encounter critical layers anywhere in the flow. The corresponding horizontal phase speed is either negative (for $\tilde{k} < 0$) or greater than $2U_0$ (for $\tilde{k} > 0$). In the region to the right of the dashed-dotted line the frequency and wave number of the internal waves are such that they encounter a critical layer. If $\mathrm{Ri}_g > 1/4$ at the critical level the waves exhibit a rapidly oscillating vertical structure. Consistent with the predictions of ray theory, it is assumed that the waves dissipate in this circumstance and so neither transmission nor reflection occurs.

The WKB approximation applies when $\tilde{m} \gg 1$. The associated range of frequencies and wave numbers lie in a small region above the line $\tilde{\omega} = 2\tilde{k}$, which corresponds to the dashed-dotted line in the four plots of Fig. 4. Because the WKB approximation is plausible over such a small region this problem requires different techniques to completely describe wave propagation and is well-posed for our numerical solver.

Figure 4(a) shows transmission coefficients for waves incident upon a highly unstable shear flow for which $\mathrm{Ri}_b = 0.001$. For $\tilde{k} < 0$, despite being Doppler-shifted to fre-

quencies close to N_0, transmission is strong for a wide range of $\tilde{\omega}$ and $\tilde{k}$. The transmission is lowest for small $\tilde{\omega}$, corresponding to incident waves with vertical wavelengths that are short compared to the horizontal wavelength but long when compared with the gap depth. To the right of the dashed-dotted line, corresponding to parameters for which waves encounter a critical layer, there is weak but nonzero transmission over nearly the entire region.

In Fig. 4(b), the transmission coefficient is plotted for $\mathrm{Ri}_b=0.01$. Although the bulk Richardson number has increased by an order of magnitude, N_0 is two orders of magnitude smaller than U_0/L so that shear effects still dominate. As such, the transmission is largely unchanged in the noncritical region. The most significant differences are apparent near $\tilde{\omega}=0$, where the transition from poor transmission to strong transmission occurs over a shorter range of $\tilde{\omega}$, and also to the left of the dashed-dotted line that separates the region between critical and noncritical transmission, where the transition from weak transmission to strong transmission occurs over a smaller range of $\tilde{k}$. In the critical region the effect of increasing Ri_b is more significant. There is a smaller region of $\tilde{\omega}$ and $\tilde{k}$ which have $\mathrm{Ri}<1/4$ at the critical layer so that the parameter range over which transmission occurs is smaller. However, because $\bar{\Omega}$ approaches zero at a critical layer, the $N^2/\bar{\Omega}^2$ term dominates the Taylor-Goldstein equation. As such, increasing N_0 by an order of magnitude significantly affects the transmission in the region that encounters a critical layer. Compared with the case where $\mathrm{Ri}_g=0.001$, there is a large increase (typically over 500%) in the transmission coefficients in the critical region.

Figure 4(c) plots the transmission coefficient for $\mathrm{Ri}_b=0.1$. Because N_0 is now only an order of magnitude smaller than U/L the buoyancy frequency has significant influence on the transmission characteristics. Comparing the noncritical transmission region to that in Figs. 4(a) and 4(b), it is apparent that the transition from relatively weak to strong transmission near $\tilde{\omega}=0$ and the $\tilde{\Omega}(z)=0$ line occurs over a smaller range of frequencies—transmission coefficients are larger than 0.5 over nearly the entire domain. In the critical region transmission is even stronger. For smaller $\tilde{\omega}$ and $\tilde{k}$ the transmission coefficient is consistently as large as 0.3 and above 0.15 over most of the range of parameters with waves that encounter a critical level.

In Fig. 4(d) transmission is plotted for relatively stable flow with $\mathrm{Ri}_b=1$. In this case N_0 is the same order of magnitude as U/L and the shear has less impact upon the wave propagation. In the limit as Ri_b approaches infinity perfect transmission is expected throughout the non-critical region and no transmission in the critical region. With $\mathrm{Ri}_b=1$ the transmission is already approaching this limit with transmission greater than 0.95 over nearly the entire range of parameters that allow wave propagation. In the critical region, to the right of the dashed-dotted line, transmission is not possible. This is because $\mathrm{Ri}_g>1/4$ over the entire critical region so that waves may not propagate across the critical layer.

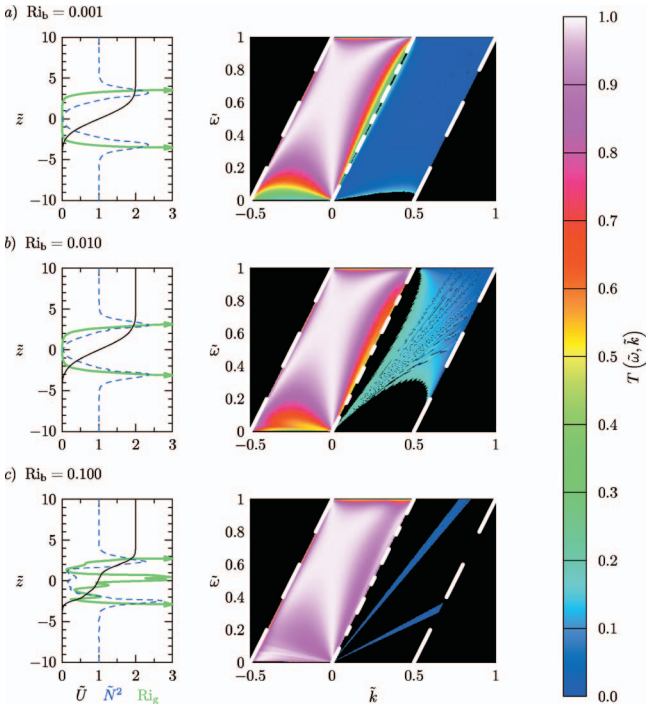

FIG. 5. (Color) Background buoyancy frequency, shear, and gradient Richardson number profiles (left panels) for an evolving shear flow at $t=100L/U_0$ and corresponding transmission contour plots (right panels) for (a) $\mathrm{Ri}_b=0.001$, (b) $\mathrm{Ri}_b=0.010$, and (c) $\mathrm{Ri}_b=0.100$. The contour range and bounding lines correspond to those in Figs. 4(a)–4(c).

V. MIXED LAYER RESULTS

The background profiles examined in the previous section are unstable for $\mathrm{Ri}_g<1/4$. In this section we consider wave transmission across a mixed layer resulting from taking the initial conditions given by Eqs. (17) and (18) and solving the Navier-Stokes equations so as to evolve the system until it reaches a quasisteady state. Explicitly, the horizontally averaged background N^2 and $\bar{U}$ profiles are determined at time $t=100L/U_0$. The code used to perform this calculation is described in detail by Sutherland and Peltier.[28]

Background shear and buoyancy frequency profiles, as well as the gradient Richardson number in the central mixed region, are plotted in the left panels of Fig. 5 for $\mathrm{Ri}_b=0.001$, 0.01, and 0.1. The circumstance with $\mathrm{Ri}_b=1$, studied in Sec. IV, is omitted as the flow is stable in this case. The evolution of the flow involves the development of Kelvin-Helmholtz billows that mix the region about $\tilde{z}=0$ both broadening the shear layer and locally reducing $\tilde{N}$. The resulting mean flow and horizontal averaged $\tilde{N}^2$ profiles are similar to the piecewise-linear profile across which transmission was considered using an analytic formula by Brown and Sutherland.[20] Not only do incident waves encounter a shear layer, but they also encounter a localized region of reduced $\tilde{N}^2$ where the waves may be evanescent. If this region is sufficiently narrow, it is nonetheless possible for waves to tunnel through. The corresponding transmission coefficients are given in the right panels of Figs. 5(a)–5(c). These are analogous to Figs. 4(a)–4(c), respectively.

When the shear is relatively weak compared to the

strength of the buoyancy frequency the resulting transmission is similar to that of the nonevolved profiles in the noncritical region. As in Sec. III we find that although there is a reflection level near $\tilde{z}=0$ where $\tilde{N}^2=0$, almost perfect transmission occurs for a wide range of $\tilde{\omega}$ and $\tilde{k}$. The similarities between the transmission contours for the evolved and original profiles suggests that internal waves transmit across the mixed region throughout the mixing process.

In the region of the plot where a critical layer is encountered (to the right of the dashed-dotted line) there are more significant differences between the transmission contours for the original and evolved profiles. The mixing induces opposing effects in the gradient Richardson number: the broadening of the shear layer acts to reduce $\bar{U}'$, thus increasing Ri_g, while the mixing reduces N, thus decreasing Ri_g. Although the effects are comparable in magnitude, Ri_g is typically larger after the fluid has mixed suggesting that the mixing in the gap is dominated by the broadening of the shear layer. As such, wave transmission is possible for a smaller range of $\tilde{\omega}$ and $\tilde{k}$ and indeed the transmission coefficient is nonnegligible over a smaller parameter range.

For $\mathrm{Ri}_b=0.001$ the shear and buoyancy frequency profiles are symmetric about $\tilde{z}=0$. This results from the fine-scale convective instability which occurs when KH billows transport dense fluid over light. In the mixed region $\mathrm{Ri}_g<1/4$ for $|\tilde{z}|<2.81$ and in this range $0.05<\tilde{U}<1.95$. As such, transmission is possible in the critical region for a very broad range of $\tilde{\omega}$ and $\tilde{k}$. In comparing transmission for the evolved and nonevolved profiles of Figs. 5(a) and 4(a), respectively, it is clear that in the critical region transmission occurs over a comparable range of $\tilde{\omega}$ and $\tilde{k}$ and that transmission is poor in both cases—the differences between the two plots are almost indistinguishable.

For $\mathrm{Ri}_b=0.01$ the differences between the original and evolved profiles are more apparent. Comparing Figs. 4(b) and 5(b) it is clear that there is generally stronger transmission of waves that do not encounter a critical level, particularly for low frequency waves. A transmission "valley" occurs for $0\lesssim\tilde{\omega}\lesssim0.1$ and $-0.5<\tilde{k}<0$ when $0.1\lesssim\tilde{\omega}/\tilde{k}\lesssim0.5$. For these profiles, $\mathrm{Ri}_g<1/4$ in the mixed region for $|\tilde{z}|<2.11$ over which range $0.18<\tilde{U}<1.82$. In the critical region slightly stronger transmission occurs compared to that computed for the original profiles, although non-negligible transmission occurs over a smaller range of parameter space for the evolved profiles.

For $\mathrm{Ri}_b=0.1$, comparing the transmission contours in Figs. 4(c) and 5(c) we see again that, in the noncritical region, transmission is generally stronger for the evolved plots and that a transmission "valley" (though weak) occurs for $0.5\lesssim\tilde{\omega}/\tilde{k}\lesssim2.3$ if $\tilde{\omega}<0.3$. In the critical region there is significant deviation from the transmission contours obtained from the original profiles. There are two small bands of (relatively weak) transmission for the evolved profiles whereas transmission was possible over a large range of parameters for the original profiles. The lower frequency transmission band coincides with waves encountering a critical level with $\mathrm{Ri}_g<1/4$ where $-2.34<\tilde{z}<-2.19$ for which $0.42<\tilde{U}<0.47$. There is a maximum in shear gradient at this level. The higher transmission band occurs for waves encountering a critical level where $1.02<\tilde{z}<1.56$ for which $1.11<\tilde{U}<1.31$. This is coincident with a minimum in buoyancy frequency. For the original profiles critical transmission was at its greatest in this case.

VI. CONCLUSIONS

We have developed a method to calculate the transmission of internal waves through fluid with arbitrarily specified density and shear profiles. We found that WKB theory accurately predicts, within 98%, near perfect transmission into unsheared, weakly stratified fluid if $\tilde{m}_1>1$. For longer vertical wavelengths, the calculated transmission is lower than the WKB prediction. Wave transmission across a uniformly stratified shear layer is found if waves do not encounter a critical layer and if they encounter a critical level where $\mathrm{Ri}_g<1/4$. The quantitative behavior is similar for internal waves propagating across a mixed region.

The method can be used in general to examine transmission through arbitrary N^2 and $\bar{U}$ profiles and could prove useful, in particular, in diagnosing transmission across the equatorial undercurrent. In future work, we intend to extend the method to include anelastic effects so that we may examine the transmission and reflection of internal waves originating in the troposphere and propagating through the mesosphere into the upper atmosphere.

APPENDIX: METHOD OF FROBENIUS

For internal waves encountering a critical layer, $\bar{\Omega}(z^*)=0$ for some z^* in the domain of the flow. As $\bar{\Omega}$ appears in the denominator of the ϕ coefficient in the Taylor Goldstein equation this results in a singularity. However, we may rewrite Eq. (2) as

$$\bar{\Omega}^2\phi''+k^2\left(N^2+\frac{\bar{U}''\bar{\Omega}}{k}-\bar{\Omega}^2\right)\phi=0, \tag{A1}$$

and, when certain criteria are met, solve using the Frobenius method.

To solve using the method of Frobenius, we must first fit polynomials to the coefficients in Eq. (A1). We make a linear fit to $\bar{\Omega}$ near the singularity at z^*:

$$\bar{\Omega}^2(z)=a(z-z^*)^2, \tag{A2}$$

and allow a parabolic fit to the ϕ coefficient

$$k^2N^2(z)+k\bar{\Omega}U''(z)-k^2\bar{\Omega}^2(z)=b(z-z^*)^2+c(z-z^*)+d, \tag{A3}$$

so that we may rewrite Eq. (A1)

$$a(z-z^*)^2\phi''(z)+[b(z-z^*)^2+c(z-z^*)+d]\phi(z)=0. \tag{A4}$$

Then, applying the method of Frobenius,[29] we assume that $\phi(z)$ has solutions of the form

$$\phi(z) = |z - z^*|^r \sum_{n=0}^{\infty} a_n (z - z^*)^n, \tag{A5}$$

where r is found from the indicial equation,

$$r = \frac{1}{2} \pm \sqrt{\frac{1}{4} - \frac{d}{a}}, \tag{A6}$$

and, as r must be real, we require that $d/a < 1/4$. This is equivalent to the requirement that Eq. (3) be less than $1/4$ at the critical level for wave transmission to occur. We then find the coefficients of the Frobenius expansion as

$$a_n = \frac{ba_{n-2} + ca_{n-1}}{a(n+r)(n+r-1) + d}. \tag{A7}$$

Using this technique, two solutions are generated, one for each r value. A superposition of these two results is chosen such that the Frobenius solution will match the Stoermer method solution at the last point of integration before the critical layer.

[1] K. L. Polzin, J. M. Toole, J. R. Ledwell, and R. W. Schmitt, "Spatial variability of turbulent mixing in the Abyssal Ocean," Science **276**, 93 (1997).

[2] J. R. Ledwell, E. Montgomery, K. Polzin, L. C. St. Laurent, R. Schmitt, and J. Toole, "Evidence for enhanced mixing over rough topography in the abyssal ocean," Nature **403**, 179 (2000).

[3] E. Firing, "Deep zonal currents in the central equatorial Pacific," J. Mar. Res. **45**, 791 (1987).

[4] T. M. Dillon, J. N. Moum, T. K. Chereskin, and D. R. Caldwell, "Zonal momentum balance at the equator," J. Phys. Oceanogr. **19**, 561 (1989).

[5] D. Hebert, J. N. Moum, C. A. Paulson, D. R. Caldwell, T. K. Chereskin, and M. J. McPhaden, "The role of the turbulent stress divergence in the equatorial Pacific zonal momentum balance," J. Geophys. Res. **96**, 7127 (1991).

[6] E. D. Skyllingstad and D. W. Denbo, "The role of internal gravity waves in the equatorial current system," J. Phys. Oceanogr. **24**, 2093 (1994).

[7] B. R. Sutherland, "The dynamic excitation of internal gravity waves in the equatorial oceans," J. Phys. Oceanogr. **26**, 3214 (1996).

[8] T. N. Palmer, G. J. Shutts, and R. Swinbank, "Alleviation of a systematic westerly bias in general circulation and numerical weather prediction models through an orographic gravity drag parametrization," Q. J. R. Meteorol. Soc. **112**, 1001 (1986).

[9] N. A. McFarlane, "The effect of orographically excited gravity wave drag on the general circulation of the lower stratosphere and troposphere," J. Atmos. Sci. **44**, 1775 (1987).

[10] Y. Yamada, H. Fukunishi, T. Nakamura, and T. Tsuda, "Breaking of small-scale gravity waves and transition to turbulence observed in OH airglow," Geophys. Res. Lett. **28**, 2153 (2001).

[11] M. Alexander, P. May, and J. Beres, "Gravity waves generated by convection in the Darwin area during the Darwin Area Wave Experiment," J. Geophys. Res. **109**, D20S04, doi: 10.1029/2004JD004729 (2004).

[12] J. B. Snively and V. P. Pasko, "Breaking of thunderstorm-generated gravity waves as a source of short-period ducted waves at mesopause altitudes," Geophys. Res. Lett. **30**, 2254 (2003)

[13] R. L. Walterscheid, G. Schubert, and D. G. Brinkman, "Small-scale gravity waves in the upper mesosphere and lower thermosphere generated by deep tropical convection," J. Geophys. Res. **106**, 31825 (2001).

[14] M. J. Lighthill, *Waves in Fluids* (Cambridge University Press, Cambridge, 1978).

[15] D. Broutman, J. W. Rottman, and S. D. Eckermann, "Ray methods for internal waves in the atmosphere and ocean," Annu. Rev. Fluid Mech. **36**, 233 (2004).

[16] R. S. Lindzen and J. W. Barker, "Instability and wave over-reflection in stably stratified shear flow," J. Fluid Mech. **151**, 189 (1985).

[17] C. Eckart, "Internal waves in the ocean," Phys. Fluids **4**, 791 (1961).

[18] D. C. Fritts and L. Yuan, "An analysis of gravity wave ducting in the atmosphere: Eckart's resonances in thermal and Doppler ducts," J. Geophys. Res. **94**, 18455 (1989).

[19] B. R. Sutherland and K. Yewchuk, "Internal wave tunnelling," J. Fluid Mech. **511**, 125 (2004).

[20] G. L. Brown and B. R. Sutherland, "Internal wave tunnelling through nonuniformly stratified shear flow," Atmos. Ocean (in press).

[21] I. A. Eltayeb and J. F. McKenzie, "Critical-level behaviour and wave amplification of a gravity wave incident upon a shear layer," J. Fluid Mech. **72**, 661 (1975).

[22] C. A. Van Duin and H. Kelder, "Reflection properties of internal gravity waves incident upon a hyperbolic tangent shear layer," J. Fluid Mech. **120**, 505 (1981).

[23] P. G. Drazin and W. H. Reid, *Hydrodynamic Stability* (Cambridge University Press, Cambridge, 1981).

[24] W. H. Press, B. P. Flannery, S. A. Teukolsky, and W. T. Vetterling, *Numerical Recipes: The Art of Scientific Computing*, 2nd ed. (Cambridge University Press, New York, 1993).

[25] A. Eliassen and E. Palm, "On the transfer of energy in stationary mountain waves," Geofys. Publ. **22**, 1 (1961).

[26] D. G. Andrews and M. E. McIntyre, "On wave action and its relatives," J. Fluid Mech. **89**, 647 (1978).

[27] J. F. Scinocca and T. G. Shepherd, "Nonlinear wave-activity conservation laws and Hamiltonian structure for the two-dimensional anelastic equations.," J. Atmos. Sci. **49**, 5 (1992).

[28] B. R. Sutherland and W. R. Peltier, "The stability of stratified jets," Geophys. Astrophys. Fluid Dyn. **66**, 101 (1992).

[29] W. E. Boyce and R. E. DiPrima, *Elementary Differential Equations and Boundary Value Problems*, 5th ed. (Wiley, New York, 1992).